PAPER

Long-Time Coherent Integration for Non-Radial Moving Target Based on Radon Fourier Transform with Modified Variant Angle

Denghui YAO[†,††a)], **Xiaoyong ZHANG**[††], **Zhengbo SUN**[††], ***Nonmembers***, ***and*** **Dexiu HU**[†], ***Member***

SUMMARY Long-term coherent integration can significantly improve the ability to detect maneuvering targets by radar. Especially for weak targets, longer integration times are needed to improve. But for non-radially moving targets, the time-varying angle between target moving direction and radar line of sight will cause non-linear range migration (NLRM) and non-linear Doppler frequency migration (NLDFM) within long-time coherent processing, which precludes existing methods that ignore angle changes, and seriously degrades the performance of coherent integration. To solve this problem, an efficient method based on Radon Fourier transform (RFT) with modified variant angle model (ARFT) is proposed. In this method, a new parameter angle is introduced to optimize the target motion model, and the NLRM and NLDFM are eliminated by range-velocity-angle joint three-dimensional searching of ARFT. Compared with conventional algorithms, the proposed method can more accurately compensate for the NLRM and NLDFM, thus achieving better integration performance and detection probability for non-radial moving weak targets. Numerical simulations verify the effectiveness and advantages of the proposed method.

key words: *long-time coherent integration, moving target detection, Radon Fourier transform, variant angle model*

1. Introduction

Radar is an important tool for detecting targets regardless of time or weather. But with the rapid development of stealth technology, maneuvering targets are becoming difficult to detect, making radar detection very problematic [1]–[6]. Fortunately, long-term coherent integration is an effective method to enhance the capability of moving target detection since it can provide the highest signal-to-noise ratio (SNR) gain [7]–[10]. However, with the increasing of integration time, the complex motions of maneuvering targets, e.g., high velocity and acceleration, will generate range migration (RM) [11]–[13] and Doppler frequency migration (DFM) [14], [15] both of which seriously degrade the performance. Therefore, effectively compensating RM and DFM has become a hot topic in the field of radar signal processing.

Moving target detection (MTD) is a simple coherent integration algorithm without the elimination of RM and DFM, but the poor performance limits the application. To correct RM, axis rotation-moving target detection (AR-MTD) [16] is proposed, which is implemented by range-velocity two-dimensional (2D) searching process. Methods adopting keystone transform (KT) [17], [18] can solve the linear RM without any prior knowledge via scaling the echo signal in the slow time domain. On this basis, the second-order KT (SKT) [19], [20] is proposed to eliminate the quadratic RM, namely, range curvature. Moreover, to resolve Doppler ambiguity, KT needs to combine transforms, i.e., Chirp-Z [21], Dechirping [22]. Radon Fourier transform (RFT) [23]–[25] utilizes Radon transform to extract the echo signal from the range-velocity plane and construct a Doppler matched filter to compensate for the RM, effectively integrating the constant velocity targets even in the case of Doppler ambiguity. In addition, generalized RFT (GRFT) [26] is the expansion of RFT for dealing with complex motion targets.

On the other hand, the algorithms on the DFM compensation, which is induced by target high-order motion, have also been sufficient in recent years. Due to the echo signal of maneuvering targets with constant acceleration can be modeled as a linear frequency modulated (LFM) signal, a wide variety of time-frequency analysis tools are employed to analyze the signal and eliminate DFM, e.g., Fractional Fourier transform (FRFT) [27], Lv's distribution (LVD) [28]. FRFT is an upgraded version of Fourier transform with the function of converting LFM signals to impulse signals, thus it has a good energy concentration property for accelerated targets. KT-FRFT [29], Radon-FrFT (RFRFT) [30], and improved AR-FRFT (IAR-FRFT) [31] are applicable for the removal of DFM. LVD is a new method for signal analysis that has been reported to provide the improved detection ability of LFM signals. KT-LVD [32] and Radon-LVD (RLVD) [33] are proposed to deal with RM and DFM.

The aforementioned methods have good performance in their respective scenes, but most of them need to suppose that the angle between the target motion direction and the radar line of sight (RLOS) remains unchanged within long-term integration when establishing the target motion model. This hypothesis obviously holds for radial moving targets. Unfortunately, the trajectory of targets strictly satisfying the radial is rare, and most targets detected by radar are moving in a non-radial direction in practice. For non-radial moving targets, the angle between its trajectory and RLOS is time-varying. More seriously, the changing angle causes the target trajectory becomes more complicated and creates non-linear RM (NLRM) and non-linear DFM (NLDFM). If the conventional methods based on the assumption of invariant angle are stubbornly utilized to deal

Manuscript received August 23, 2021.
Manuscript revised October 15, 2021.
Manuscript publicized November 9, 2021.

[†]The authors are with Information Engineering University, Zhengzhou, China.
[††]The authors are with National Key Laboratory on Blind Signal Processing, Chengdu, China.
a) E-mail: yao_dh@126.com

DOI: 10.1587/transcom.2021EBP3136

with non-radial moving targets, it will mismatch the model between target and algorithm, inevitably failing to eliminate NLRM and NLDFM and degrading the performance of integration. In order to keep the algorithm working properly, the current methods have no choice but to perform under a limited time in which the angle approximately maintains constant. But this way of sacrificing integration time leads to an irreconcilable contradiction between integration time and integration gain. On the one hand, the time must be increased to improve gain for detecting the weak targets. On the other hand, the increase in time will produce more serious NLRM and NLDFM, which cause gain to decrease.

To solve the above problems, this paper proposes a method based on RFT with a modified variant angle (ARFT) to compensate for the NLRM and NLDFM. As we know, RFT-based algorithms have been studied extensively, and some modified RFT methods have been recently proposed in the existing literature. Unfortunately, they did not consider the impact of angle change on long-term coherent integration and the incorrect motion model was used for dealing with NLRM and NLDFM. Thus, the proposal and application of the ARFT are significant for the long-time coherent integration of non-radial moving targets, which is very common in practice. In this method, the angle between the target motion direction and RLOS is set as a new parameter to modify the target motion model. Then the two-dimensional (2D) search with range-velocity of RFT is expanded to three-dimensional (3D) search with the range-velocity-angle. Simulation results validate the effectiveness of the proposed method for non-radial moving target integration and detection.

This paper is organized as follows. Section 2 establishes the signal model. Section 3 introduces the principle of the proposed method. Then, Sect. 4 gives a series of numerical simulations. Finally, Sect. 5 concludes this paper.

2. Signal Model and Problem Formulation

Suppose that the radar transmits a LFM signal, which can be written as:

$$s_t(t_k, t_m) = \mathrm{rect}\left(\frac{t_k}{t_p}\right)\exp(j\pi K t_k^2)\exp\left[j2\pi f_c(t_k + t_m)\right], \tag{1}$$

where,

$$\mathrm{rect}\left(\frac{t}{t_p}\right) = \begin{cases} 1, & |t| \le t_p/2 \\ 0, & |t| \ge t_p/2 \end{cases}, \tag{2}$$

is the rectangular window function, t_k represents fast time, t_p denotes the pulse duration, $t_m = m\mathrm{PRT}$ ($m = 1, 2, \ldots, M$) denotes slow time, PRT denotes the pulse repetition time and M is integration pulses number. K denotes the frequency modulated rate, f_c denotes the carrier frequency. Thus, the mth pulse echo signal scattered from the target received by the radar after down-conversion can be stated as:

$$s_r(t_k, t_m) = A_0 rect\left[\frac{t_k - \frac{2R(t_m)}{c}}{t_p}\right]\exp\left\{j\pi K\left[t_k - \frac{2R(t_m)}{c}\right]^2\right\} \times \exp\left[-j2\pi f_c\frac{2R(t_m)}{c}\right], \tag{3}$$

where A_0 is the target reflectivity, c is the speed of light, $R(t_m)$ is the instantaneous slant range between the radar and target. Use match filter $h(t_k) = rect\left(\frac{t_k}{t_p}\right)\exp\left(j\pi K t_k^2\right)$ and according to stationary phase principle, the signal after pulse compression (PC) in the range-Doppler domain can be expressed as:

$$s_{pc}(t_k, t_m) = A_1\mathrm{sinc}\left[B\left(t_k - \frac{2R(t_m)}{c}\right)\right]\exp\left[-\frac{j4\pi f_c R(t_m)}{c}\right], \tag{4}$$

where A_1 is the amplitude after PC, B is the signal bandwidth.

It can be seen from Eq. (4) that $R(t_m)$ will produce migration on envelope and phase of the signal. Therefore, in order to effectively compensate RM and DFM, the first step of coherent integration algorithm is accurately estimating $R(t_m)$ and it is directly determined by the target motion model. This paper primarily discusses the effect of varying flight angles on the target motion model but does not make specific requirements for the target motion state. Therefore, the most unadorned uniform linear motion model is selected to calculate $R(t_m)$.

Consider the scenario of target integration and detection shown in Fig. 1, a target moves with uniform speed v_0 along the non-radial direction and the initial radial slant range between target and radar is R_0, the initial angle between target motion direction and RLOS is θ_0, and the integration time is t_m. Hence, according to the conventional algorithm, the $R(t_m)$ can be calculated as:

$$R(t_m) = R_0 - v_0\cos\theta_0 t_m, \tag{5}$$

then we can employ Eq. (5) to compute:

$$\mathrm{RM} = -v_0\cos\theta_0 t_m, \mathrm{DFM} = 0. \tag{6}$$

From Eq. (5), we can see clearly that the angle is set to constant during coherent integration. Nevertheless, the

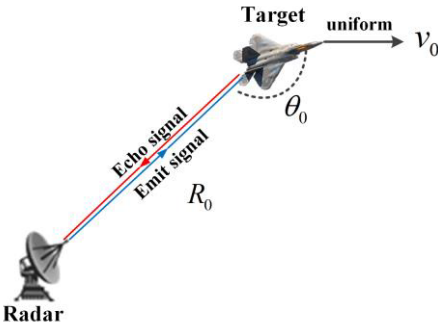

Fig. 1 Non-radial moving targets scenario.

angle is changing, and it satisfies:

$$\theta = \arccos \frac{2R_0 v_0 t_m \cos\theta_0 - 2v_0^2 t_m^2}{2v_0 t_m \sqrt{R_0^2 + (v_0 t_m)^2 - 2R_0 v_0 t_m \cos\theta_0}}. \quad (7)$$

It is apparent that the angle is time varying and is related to R_0, v_0, and θ_0. What is more, $R(t_m)$ varies nonlinearly with t_m and produces NLRM and NLDFM, which are inconsistent with the calculation of Eq. (5) and Eq. (6). Thus, when dealing with non-radial moving targets, the current methods have errors in calculating $R(t_m)$ due to the wrong assumption, and the uncompensated NLRM and NLDFM will bring significant problems to coherent integration.

3. Coherent Integration Based on ARFT

In this section, a method called ARFT is proposed to realize the coherent integration for non-radial moving targets.

3.1 Variant Angle Model

As the analysis in Sect. 2, we know that the non-radial moving targets generate NLRM and NLDFM and inevitably impact the performance of conventional methods. To address this problem, we introduce a modified motion model with a variant angle and the geometric diagram as shown in Fig. 2.

In this model, the angle namely $\theta(t_m)$ is set as a new parameter which is varying with t_m during integration. Thus, we can use the cosine theorem to rewrite the equations of $R(t_m)$ as:

$$R(t_m) = \sqrt{R_0^2 + (v_0 t_m)^2 - 2R_0 v_0 t_m \cos\theta_0}, \quad (8)$$

then RM and DFM are derived as follows:

$$\begin{aligned} \mathrm{RM} &= \sqrt{R_0^2 + (v_0 t_m)^2 - 2R_0 v_0 t_m \cos\theta_0} - R_0, \\ \mathrm{DFM} &= \frac{2v_0 \left[\cos\theta(t_m) - \cos\theta_0\right]}{\lambda}, \end{aligned} \quad (9)$$

λ is signal wavelength. Compared with the traditional model, Eq. (8) and Eq. (9) match the real motion of the target. Hence, $R(t_m)$ can be estimated more accurately thanks to the introduction of $\theta(t_m)$ and it makes preparation for correction of NLRM and NLDFM.

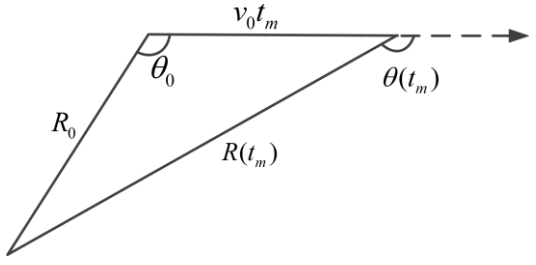

Fig. 2 Modified variant angle model for non-radial moving targets.

3.2 Correction and Integration

After optimizing the target motion model using variant angle, we apply Eq. (8) into Eq. (4) produce:

$$\begin{aligned} &s_{pc}(t_k, t_m) = \\ &A_1 \mathrm{sinc}\left[B\left(t_k - \frac{2\sqrt{(R_0)^2 + (v_0 t_m)^2 - 2R_0 v_0 t_m \cos\theta_0}}{c}\right)\right] \\ &\exp\left[-j\frac{4\pi\sqrt{(R_0)^2 + (v_0 t_m)^2 - 2R_0 v_0 t_m \cos\theta_0}}{\lambda}\right]. \end{aligned} \quad (10)$$

The NLRM and NLDFM showed in Eq. (10) must be corrected to realize coherent integration. Inspired by RFT which utilizes 2D searching of range-velocity to compensate RM and DFM, we consider the method of multidimensional unknown motion parameters searching, extracting target envelope and constructing filter array to deal with NLRM and NLDFM. Precisely for this problem, it is obvious that $R(t_m)$ relates to R_0, v_0, and θ_0. Thus, except R_0, v_0 which have been taken into account in original RFT, it must also add the search of θ_0 on this basis to describe $R(t_m)$ in Eq. (8) more precisely. Note that the range-velocity 2D searching of RFT should be promoted to range-velocity-angle 3D searching, and we called the modified RFT with the search of angle ARFT. The process of ARFT can be formulated as follow:

$$\begin{aligned} &G(r, v, \theta) = \\ &\int_0^T \int_0^{t_p} s_{pc}(t_k, t_m)\, \delta\left[t_k - \frac{2\sqrt{r^2 + (vt_m)^2 - 2rvt_m\cos\theta}}{c}\right] \\ &H_{rv\theta}(t_m)\, dt_k dt_m, \end{aligned} \quad (11)$$

where G denotes the coherent integration result of ARFT, T is total integration time, r, v, and θ are the search value of the initial range, velocity and angle respectively, $\delta(t)$ is the impulse function and $H_{rv\theta}(t_m)$ represents Doppler filter function which is defined as:

$$H_{rv\theta}(t_m) = \exp\left[\frac{j4\pi\sqrt{R_0^2 + (v_0 t_m)^2 - 2R_0 v_0 t_m \cos\theta_0}}{\lambda}\right]. \quad (12)$$

As shown in Eq. (11), $\delta(t_k)$ serves to extract the target from the fast time-slow time domain and concentrate signal energy into one range cell, which can estimate NLRM. On the other hand, $H_{rv\theta}(t_m)$ plays a role in compensating the phase fluctuation, which can correct NLDFM. Therefore, ARFT is implemented by search within a specific scope and only when $r = R_0$, $v = v_0$, $\theta = \theta_0$, NLRM and NLDFM are completely compensated, and the maximum value of coherent integration $G_{\max} = A_1 T$ is obtained.

In addition, the search scope and interval of target unknown motion parameters are crucial for the effective implementation of ARFT. Generally, the search scope is determined by the radar detection task. Assuming that the

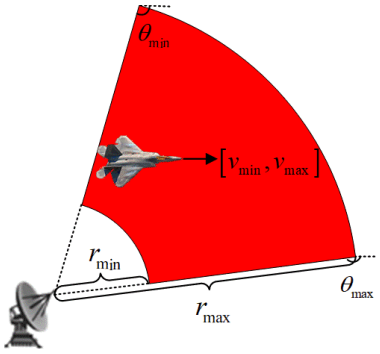

Fig. 3 Sketch map of parameter search scope.

task of the radar is to detect the target within the red sector area in Fig. 3, the search scope of ARFT is $r \in [r_{\min}, r_{\max}]$, $v \in [v_{\min}, v_{\max}]$, $\theta \in [\theta_{\min}, \theta_{\max}]$.

While the search interval is related to the signal and system parameters, specifically, the range search interval $\Delta r = \frac{c}{2f_s}$, f_s is the signal sampling frequency; the velocity search interval $\Delta v = \frac{\lambda}{2T}$; the angle search interval sets as 3 dB beam width of antenna, $\Delta\theta = 0.89\frac{\lambda}{D}$, where D is the antenna aperture. Then, the range, velocity, and angle search amount N_r, N_v, N_θ can be calculated as follows:

$$N_r = \text{round}\left(\frac{r_{\max} - r_{\min}}{\Delta r}\right), N_v = \text{round}\left(\frac{v_{\max} - v_{\min}}{\Delta v}\right),$$
$$N_\theta = \text{round}\left(\frac{\theta_{\max} - \theta_{\min}}{\Delta\theta}\right), \tag{13}$$

where round$(\ )$ denotes the integer operator.

Thus, ARFT can be further expressed as:

$$\begin{aligned} G_{ARFT} &= \max_{r,v,\theta} \int_0^T s_{pc}\left[\frac{2\sqrt{r^2 + (vt_m)^2 - 2rvt_m\cos\theta}}{c}, t_m\right] \\ &H_{rv\theta}(t_m)\, dt_m, \\ &r = r_{\min} + n_r\Delta r, \quad n_r = 1, 2, \ldots, N_r. \\ &v = v_{\min} + n_v\Delta v, \quad n_v = 1, 2, \ldots, N_v. \\ &\theta = \theta_{\min} + n_\theta\Delta\theta, \quad n_\theta = 1, 2, \ldots, N_\theta. \end{aligned} \tag{14}$$

The flowchart of the ARFT can be summarized as shown in Fig. 4:

According to the analysis, ARFT is one of the optimized coherent integration methods of RFT. Like RFT-based methods, ARFT also extracts echo signals from the fast time-slow time domain via parameters searching, but the target motion model is different. Hence, it is necessary to make a comparison between ARFT and RFT-based methods.

We can reconsider Eq. (8) and take Taylor series expansion of it:

$$R(t_m) = R_0 - v_0\cos\theta_0 t_m + \frac{v_0^2\left(1-\cos^2\theta\right)}{2R_0}t_m^2 + \sum_{n=3}\frac{R'^{(n)}(0)}{n!}t_m^n, \tag{15}$$

on the contrary, RFT calculate the $R(t_m)$ as Eq. (5). And

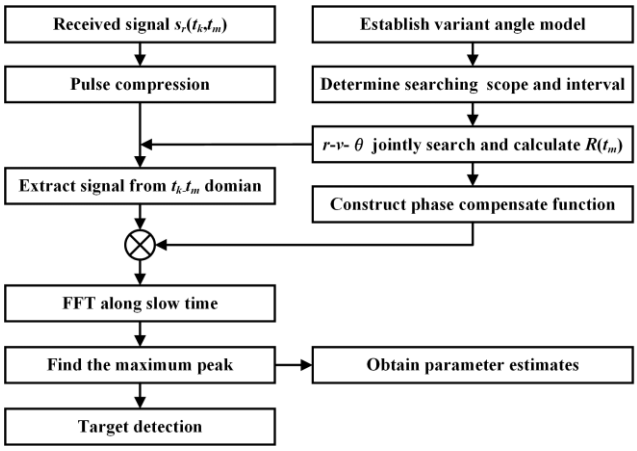

Fig. 4 Flowchart of the proposed method.

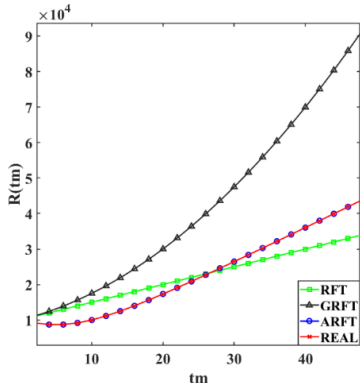

Fig. 5 Extraction results of RFT, GRFT, ARFT and real target trajectory.

second-order algorithm i.e., GRFT calculate the $R(t_m)$ as:

$$R(t_m) = R_0 - v_0\cos\theta_0 t_m + \frac{1}{2}a_0\cos\theta_0 t_m^2, \tag{16}$$

where $a_0 = v_0^2/R_0$ is target acceleration. Different models make different results of signal extraction. For comparative analysis, we set a non-radial moving target with, $R_0 = 100$ km, $v_0 = 1000$ m/s, $\theta_0 = 120°$, and the extraction results of RFT, GRFT, ARFT and the real target trajectory are shown in Fig. 5:

We can see that RFT and GRFT respectively use a line and parabola to extract signals inconsistent with the target real motion state, while ARFT applies a curve with the angle to extract signal correctly. Similarly, the phase compensation functions of RFT and GRFT also have errors, while ARFT can accurately match the target phase. This theoretically explains why the proposed algorithm is more universal for non-radial moving targets than other RFT-based algorithms.

3.3 Coherent Integration Time Comparison

We can obviously find that Eq. (5) and Eq. (16) are first-order and second-order expressions of Eq. (15) after ignoring the higher-order term. This simplification must have

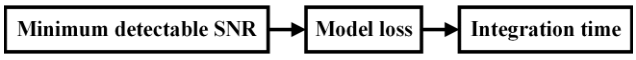

Fig. 6 Limitation of integration time.

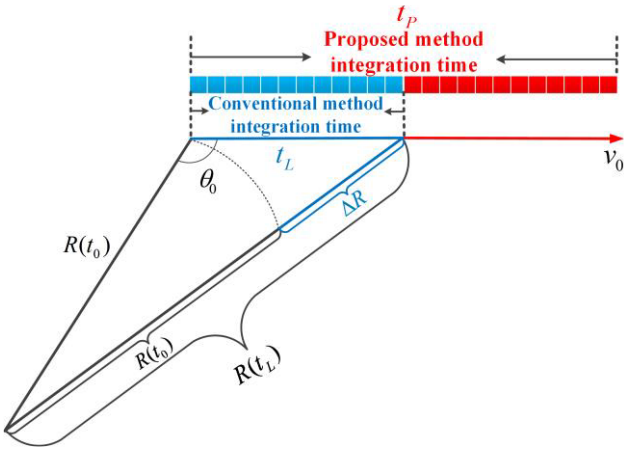

Fig. 7 Comparison of coherent integration time.

approximation errors, which inevitably provoke the loss in coherent integration, we call it model loss, namely L. Assuming that the initial SNR is S_0 and the gain of coherent integration is g. Thus, the output SNR is $S_0 + g - L$. To successfully detect the target, $S_0 + g - L \geq D_0$ must be met, where D_0 is minimum detectable SNR. In other words, there must be:

$$L \leq S_0 + g - D_0. \tag{17}$$

Unfortunately, L increases with integration time, and when it cannot satisfy the Eq. (17), target detection will fail. Therefore, the integration time constraint relationship can be summarized as Fig. 6:

Note that D_0 determines the maximum allowed value of L, and L limits the maximum integration time. What is more, we discuss the scene in Fig. 7:

As shown in Fig. 7, a target is moving at a uniform speed v, $R(t_0)$ and $R(t_m)$ respectively denote the initial and instantaneous slant range between the radar and target, $\Delta R = R(t_m) - (R_0 + v_0 t \cos\theta_0)$ is the approximate errors of conventional methods, i.e., RFT and GRFT. $\Delta R_{\max}$ is the maximum tolerable, which must obey $\Delta R \leq \Delta R_{\max}$ at any time. Thus, when $\Delta R_{\max}$ is determined, then the maximum integration time, namely t_L is determined. Accordingly, as shown in Fig. 7, the maximum coherent integration time of conventional methods is limited to t_L. On the contrary, the proposed algorithm can coherently integrate t_P. Although like t_L, both of them are limited by the target motion state, and the integration time will be shortened when the target no longer maintains a uniform linear motion. But t_P is not limited by the variation of flight angle, thus it is significantly longer than t_L.

Table 1 Comparison of computational complexities.

Methods	Computation Complexity	Search Dimension
RFT	$O(N_r N_v M)$	2-D search
GRFT	$O(N_r N_v N_a M)$	3-D search
ARFT	$O(N_r N_v N_\theta M)$	3-D search

Table 2 Simulation parameters.

Parameters	Value
Carrier frequency	1.5 GHz
Bandwidth	10 MHz
Sample frequency	20 MHz
Pulse repetition frequency	1000 Hz
Pulse duration	50 μs
Initial range	100.5 km
Initial velocity	1000 m/s
Initial angle	95.71°
Integration time	4 s
SNR after pulse compression	-20 dB

3.4 Computational Complexity Analysis

Assume that N_r, N_v, N_a, N_θ, M respectively represent the number of searching range, searching velocity, searching acceleration cells, searching angle, and integration pulses number. The computational complexities of RFT, GRFT, and the proposed method are analyzed in Table 1.

Table 1 illustrates that the proposed ARFT has comparable computational complexity to GRFT since they are both 3-D parameters search. Compared with ARFT and GRFT, the computational complexity of RFT is lower since it only performs 2-D searching. Thus, the proposed method has no superiority in terms of computation.

4. Numerical Experiments

In this section, several numerical simulations are conducted to analyze the coherent integration performance and detection probability of the proposed method for a maneuvering target with uniform velocity in a non-radial direction under the Gaussian noise environment. The results of MTD, RFT, and GFRT are also given for comparison.

4.1 Coherent Integration for Weak Target

To begin with, we evaluate the coherent integration for a weak target, where the simulation parameters are given in Table 2.

Figure 8(a) shows the signal after pulse compression, illustrating that the target is completely buried in the noise. To clearly show the target's trajectory, the signal after pulse compression without noise is given in Fig. 8(b), and it can be seen that serious NLRM is due to the high speed and variant angle. Without eliminating NLRM and NLDFM, MTD fails to detect the target, which is shown in Fig. 8(c). Moreover, the coherent integration results of RFT and GRFT,

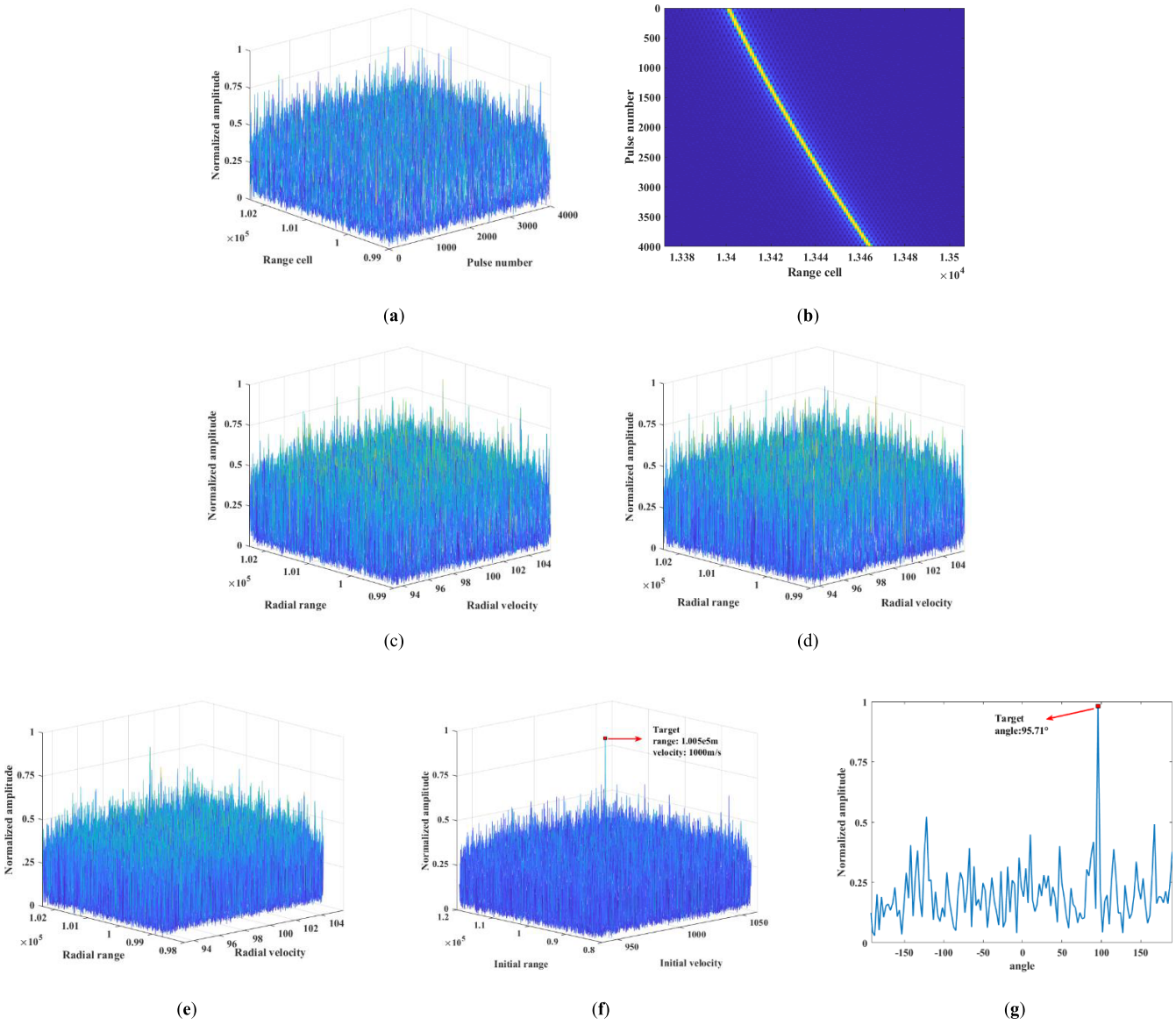

Fig. 8 Coherent integration for a weak target via MTD, RFT, GRFT, and ARFT. (a) Result after pulse compression. (b) Result after pulse compression without noise. (c) MTD (d) RFT (e) GRFT (f) ARFT in range-velocity domain (g) ARFT in angle domain.

respectively shown in Fig. 8(d) and Fig. 8(e), are ineffective due to integration loss caused by the mismatch between model and target. Instead, Fig. 8(f) and Fig. 8(g) show the result of the proposed method in range-velocity dimensions ($\theta_0 = 95.71°$) and angle dimension ($r_0 = 100.5$ km, $v_0 = 1000$ m/s), respectively. We can obviously find that the target energy is coherently integrated as one remarkable peak, which implies better coherent integration ability for weak targets.

4.2 Coherent Integration for Multiple Targets

When detecting multiple targets, ARFT adopts an iterative solution based on Eq. (14), and the specific operations are as follows:

(1) The first target result is obtained by searching the maximum value according to the ARFT algorithm, and the detection is completed combined with Constant False-Alarm Rate (CFAR) detector for detection. (2) The first target is removed from the search grid, and then ARFT is used to search the next target. CFAR is also used for detection. (3) Repeat the above process until there is no target in the CFAR detector result, and it is considered that multiple targets detection has been completed.

To prove the validity of the proposed method for multiple targets' coherent integration, two non-radial moving targets are analyzed in the experiment, and the motion parameters of the targets are listed in Table 3. To prove the validity of the proposed method for multiple targets' coherent integration, two non-radial moving targets are analyzed

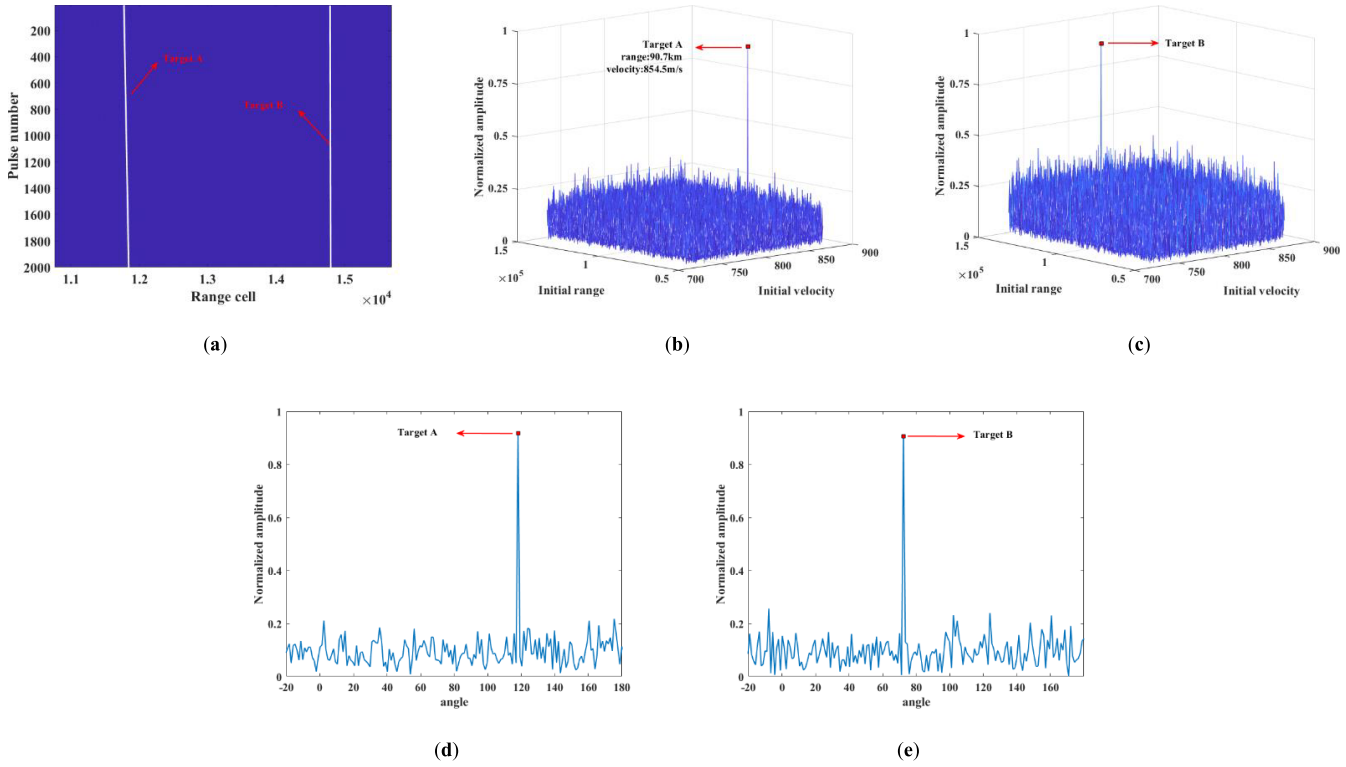

Fig. 9 Coherent integration for a weak target via MTD, RFT, GRFT, and ARFT. (a) Result after pulse compression. (b) Result after pulse compression without noise. (c) MTD (d) RFT (e) GRFT (f) ARFT in range-velocity domain (g) ARFT in angle domain.

Table 3 Motion parameters of targets.

Motion Parameters	Target A	Target B
Initial slant range	90.7 km	108.7 km
Initial velocity	854.5 m/s	764.5 m/s
Initial angle	118.1 °	72.2 °

in the experiment and the motion parameters of the targets are listed in Table 3.

Figure 9(a) shows the result after pulse compression. Besides, Fig. 9(b) and Fig. 9(c) respectively show the range-velocity search results of target A and target B via ARFT. We can clearly see targets emerge from the noise and form two sharp peaks, which are helpful for target detection. As shown in Fig. 9(d) and Fig. 9(e), two obvious peaks appear in the corresponding angle domain and demonstrate the availability of the proposed method for multiple targets. What is more, the peak values indicate the estimated motion parameters of target A and target B equal to simulation settings.

4.3 Targets Detection Ability

Furthermore, the target detection ability of MTD, RFT, GRFT, and proposed ARFT have been investigated by Monte Carlo trials. Complex white Gaussian noise with zero mean is added to the signal after pulse compression to yield SNRs varying from −25 dB to 15 dB. And for each SNR value, 1000 simulations are performed. We combine the CFAR detectors and the four methods as corresponding detectors. Besides, the false alarm ratio is set as $P_{fa} = 10^{-2}$. Other parameters are the same as Table 2 and the integration time is 1 s. The curves of detection probability (P_d) are shown in Fig. 10.

According to the results, for $P_d > 90\%$, the needed minimum SNR of MTD, RFT, GRFT, and ARFT is respectively 10 dB, 6 dB, −15 dB, −20 dB. Thus, other methods suffer from obvious detection performance loss compared to the proposed method. Moreover, when SNR=−19 dB, the of MTD, RFT, GRFT, and ARFT are respectively 1%, 1%, 14%, and 97%. Hence, it is apparent that the proposed ARFT is superior to MTD, RFT, and GRFT when dealing with non-radial moving targets due to its variant angle model to solve the NLRM and NLDFM.

4.4 Performance Analysis in Different Scenarios

As discussed above, the NLRM and NLDFM are related to the integration time, target velocity, and initial angle. Thus, in the following subsection, we separately change time, velocity, angle and analyze the detection probability of the RFT, GRFT, and ARFT to compare the stability and robustness under different conditions. Monte Carlo experiments are conducted and for each value, 1000 independent simulations are performed. Parameters of radar are given in Table 2 and the SNR after pulse compression is −20 dB.

First, curves in Fig. 11 show the result of the three

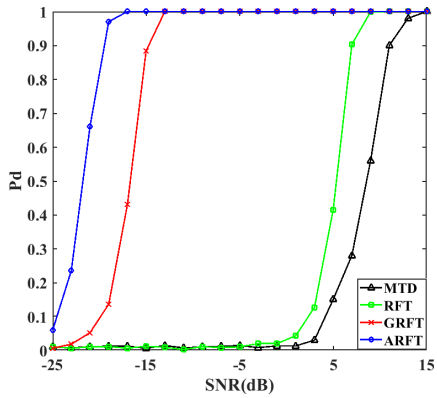

Fig. 10 Detection probability varying with SNRs.

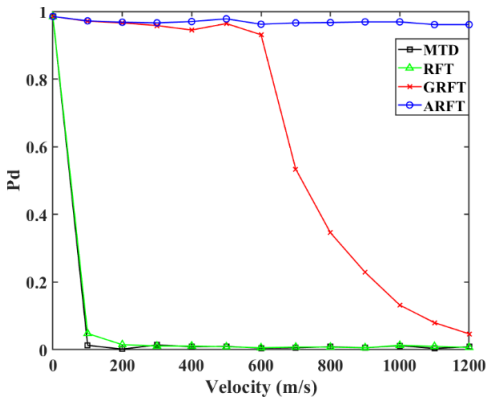

Fig. 12 Detection probability varying with target velocities.

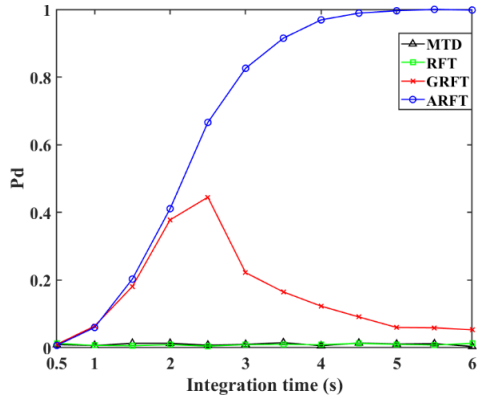

Fig. 11 Detection probability varying with integration times.

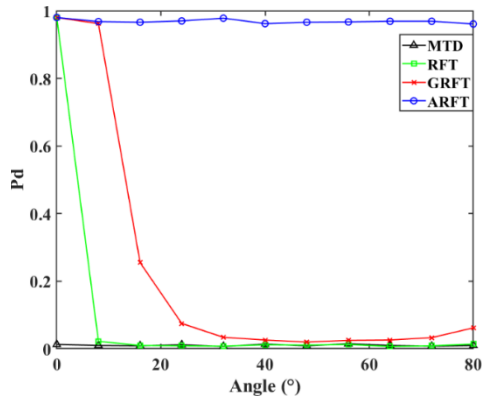

Fig. 13 Detection probability varying with initial angles.

methods under different integration times, which vary from 0.5 to 5 s. Note that the initial range, initial velocity, and initial angle of the non-radial moving target are 100.5 km, 1000 m/s, and 95.71°. It can be seen that the performance of RFT and GRFT is close to ARFT since the beginning. Nevertheless, when the time rises to a certain degree, they do not increase but fall rapidly. This is because their models have integration loss which is more severe with the increase of time, reflecting the time limitation of the conventional methods for long-time integration of non-radial moving targets. In contrast, the P_d of ARFT steadily improves with integration time thanks to the modification of the model.

Next, we evaluate the detection ability varies with initial target velocities, and the result is shown in Fig. 12. In addition, the initial range and initial angle of the non-radial moving target are 100.5 km, 95.71° and the integration time is 1 s. From Fig. 12, we can see that when $v_0 = 0$, the four methods have identical performance because a stationary target does not cause NLRM and NLDFM. While, with the increase of velocity, MTD, RFT, and GRFT decrease successively due to the unprocessed NLRM and NLDFM. On the other hand, the P_d of ARFT is consistently above 95%, maintaining good performance.

Finally, Fig. 13 shows that the fluctuation of P_d varies with angles. Besides, the initial range and initial angle of the non-radial moving target are 100.5 km, 95.71° and the integration time is 1 s. It is obvious that P_d of MTD is almost zero, while RFT, GRFT are close to ARFT at first, whereas they suddenly drop with the increase of angle. On the contrary, P_d of ARFT stables at a high level. This is because when the angle is slight, the target motion model can be regarded as a radial model. Furthermore, the NLRM and NLDFM are approximately RM and DFM, thus RFT and GRFT can be effectively performed. Unfortunately, as the angle increases, these methods are gradually invalid.

Consequently, through the above three groups of experiments, it is proved that the ARFT has good stability and practicability for detecting non-radial moving targets.

5. Conclusions

To address the NLRM and NLDFM induced by non-radial moving targets, this paper proposed a method called ARFT. Specifically, ARFT modified the target motion model via changing the angle between target motion direction and RLOS from original constant to variable and adopted motion parameters searching of range-velocity-angle based on RFT to compensate for the NLRM and NLDFM. Compared with conventional methods, i.e., MTD, RFT, and GRFT, the proposed method can: (a) achieve more satisfactory integration performance for weak targets because the limitation of integration time has been eliminated by the introduction of

variant angle; (b) obtain better target detection ability for non-radial moving targets due to the precise and meticulous motion model. Meanwhile, the simulation results demonstrated the availability of the proposed method. Moreover, we will focus on the long-time coherent integration of maneuvering non-radial moving targets with acceleration or curve trajectory in the subsequent work.

Acknowledgments

This work was supported by the National Key Laboratory of China under Grant No. 614241300206, the National Natural Science Foundation of China under Grant 62071490, and the Natural Science Outstanding Youth of Henan province under Grant 212300410095.

References

[1] K.-T. Jung and H.-M. Kim, "Performance analysis of generalized order statistic cell averaging CFAR detector with noncoherent integration," IEICE Trans. Fundamentals, vol.E81-A, no.6, pp.1201–1209, June 1998.
[2] I. Bekkerman and J. Tabrikian, "Target detection and localization using MIMO radars and sonars," IEEE Trans. Signal Process., vol.54, no.10, pp.3873–3883,2006.
[3] B. Alireza and A.M. Seyed, "Moving target detection and tracking using edge features detection and matching (pattern recognition)," IEICE Trans. Inf. & Syst., vol.E86-D, no.12, pp.2764–2774, Dec. 2003.
[4] T.W. Bae, Y.C. Kim, S.H. Ahn, and K.I. Sohng, "A novel Two-Dimensional LMS (TDLMS) using sub-sampling mask and step-size index for small target detection," IEICE Electron Express, vol.7, no.3, pp.112–117, 2010.
[5] X. Li, L. Kong, G. Cui, and W. Yi, "A low complexity coherent integration method for maneuvering target detection," Digit. Signal Process., vol.49, pp.137–147, 2016.
[6] J. Zhang, T. Su, J. Zheng, and X. He, "Novel fast coherent detection algorithm for radar maneuvering target with jerk motion," IEEE J. Sel. Topics Appl. Earth Observ., vol.10, no.5, pp.1792–1803, 2017.
[7] P. Huang, X. Xia, G. Liao, Z. Yang, and Y. Zhang, "Long-time coherent integration algorithm for radar maneuvering weak target with acceleration rate," IEEE Trans. Geosci. Remote Sens., vol.57, no.6, pp.3528–3542, 2019.
[8] J. Zhang, T. Ding, and L. Zhang, "Longtime coherent integration algorithm for high-speed maneuvering target detection using space-based bistatic radar," IEEE Trans. Geosci. Remote Sens., vol.60, pp.1–16, 2022.
[9] M. Tian, G. Liao, S. Zhu, Y. Liu, X. He, and Y. Li, "Long-time coherent integration and motion parameters estimation of radar moving target with unknown entry/departure time based on SAF-WLVT," Digit. Signal Process., vol.107, p.102854, 2020.
[10] X. Chen, J. Guan, W. Chen, L. Zhang, and X. Yu, "Sparse long-time coherent integration-based detection method for radar low-observable manoeuvring target," IET Radar, Sonar & Navigation, vol.14, no.4, pp.538–546, 2020.
[11] R. Lanari, "A new method for the compensation of the SAR range cell migration based on the chirp z-transform," IEEE Trans. Geosci. Remote Sens., vol.33, no.5, pp.1296–1299, 1995.
[12] L. Kong, X. Li, G. Cui, W. Yi, and Y. Yang, "Coherent integration algorithm for a maneuvering target with high-order range migration," IEEE Trans. Signal Process., vol.63, no.17, pp.4474–4486, 2015.
[13] X. Fang, R. Min, Z. Cao, and Y. Pi, "High-order RM and DFM correction method for long-time coherent integration of highly maneuvering target," Signal Process., vol.162, pp.221–233, 2019.
[14] S. Kageme, Y. Fukuma, T. Hara, and T. Inaba, "Verification of target detection performance improvement algorithm by coherent integration of range-profile," IEICE Technical Report, vol.109, 2009.
[15] T. Hara, "Coherent integration method of frequency division MIMO radar using the chirp Z-transform for a moving target," IEICE Technical Report, vol.117, 2018.
[16] X. Rao, H. Tao, J. Su, X. Guo, and J. Zhang, "Axis rotation MTD algorithm for weak target detection," Digit Signal Process., vol.26, pp.81–86, 2014.
[17] R.P. Perry, R.C. Dipietro, and R.L. Fante, "SAR imaging of moving targets," IEEE Trans. Aerosp. Electron. Syst., vol.35, no.1, pp.188–200, 1999.
[18] P. Huang, G. Liao, Z. Yang, X.G. Xia, J. Ma, and J. Ma, "Long-time coherent integration for weak maneuvering target detection and high-order motion parameter estimation based on keystone transform," IEEE Trans. Signal Process., vol.64, no.15, pp.4013–4026, 2016.
[19] D. Kirkland, "Imaging moving targets using the second-order keystone transform," IET Radar, Sonar & Navigation, vol.5, no.8, pp.902–910, 2011.
[20] T. Jing, W. Cui, X.G. Xia, and S.L. Wu, "Parameter estimation of ground moving targets based on SKT-DLVT processing," IEEE Trans. Comput. Imaging, vol.2, no.1, pp.13–26, 2016.
[21] D. Zhu, Y. Li, and Z. Zhu, "A keystone transform without interpolation for SAR ground moving-target imaging," IEEE Geosci. Remote Sens. Lett., vol.4, no.1, pp.18–22, 2007.
[22] J. Su, M. Xing, G. Wang, and Z. Bao, "High-speed multi-target detection with narrowband radar," IET Radar Sonar & Navigation, vol.4, no.4, pp.595–603, 2010.
[23] J. Xu, J. Yu, Y.N. Peng, and X.G. Xia, "Radon-Fourier transform for radar target detection, I: Generalized Doppler filter bank," IEEE Trans. Aerosp. Electron. Syst., vol.47, no.2, pp.1186–1202, 2011.
[24] J. Xu, J. Yu, Y.N. Peng, and X.G. Xia, "Radon-Fourier transform for radar target detection (II): Blind speed sidelobe suppression," IEEE Trans. Aerosp. Electron. Syst., vol.47, no.4, pp.2473–2489, 2011.
[25] Y. Ji, X. Jia, Y.N. Peng, and X.G. Xia, "Radon-Fourier transform for radar target detection (III): Optimality and fast implementations," IEEE Trans. Aerosp. Electron. Syst., vol.48, no.2, pp.991–1004, 2012.
[26] J. Xu, X. Xia, S. Peng, J. Yu, Y. Peng, and L. Qian, "Radar maneuvering target motion estimation based on generalized radon-Fourier transform," IEEE Trans. Signal Process., vol.60, no.12, pp.6190–6201, 2012.
[27] L.B. Almeida, "The fractional Fourier transform and time-frequency representations," IEEE Trans. Signal Process., vol.42, no.11, pp.3084–3091, 1994.
[28] X. Lv, G. Bi, C. Wan, and M. Xing, "Lv's distribution: Principle, implementation, properties, and performance," IEEE Trans. Signal Process., vol.59, no.8, pp.3576–3591, 2011.
[29] L. Dong, M. Zhan, H. Liu, L. Yong, and G. Liao, "A robust translational motion compensation method for ISAR imaging based on keystone transform and fractional fourier transform under low SNR environment," IEEE Trans. Aerosp. Electron. Syst., vol.53, no.5, pp.2140–2156, 2017.
[30] X. Chen, G. Jian, N. Liu, and H. You, "Maneuvering target detection via radon-fractional fourier transform-based long-time coherent integration," IEEE Trans. Signal Process., vol.62, no.4, pp.939–953, 2014.
[31] X. Rao, H. Tao, J. Su, X. Jian, and X. Zhang, "Detection of constant radial acceleration weak target via IAR-FRFT," IEEE Trans. Aerosp. Electron. Syst., vol.51, no.4, pp.3242–3253,2015.
[32] X. Li, G. Cui, Y. Wei, and L. Kong, "Manoeuvring target detection based on keystone transform and Lv's distribution," IET Radar Sonar & Navigation, vol.10, no.7, pp.1234–1242, 2016.
[33] X. Li, G. Cui, W. Yi, and L.J. Kong, "Coherent integration for maneuvering target detection based on radon-Lv's distribution," IEEE Signal Process. Lett., vol.22, no.9, pp.1467–1471, 2015.

Denghui Yao received the B.S. degree from the University of Electronic Science and Technology of China, in 2019 and he is currently pursuing the M.S. degree in Information Engineering University. His research interests include radar detection and signal processing.

Xiaoyong Zhang received the Ph.D. degree from the National Key Laboratory of Science and Technology on Blind Signal Processing, in 2011. His research interests include radar detection and signal processing.

Zhengbo Sun received the B.S. degree from the University of Electronic Science and Technology of China, in 2019 and he is currently pursuing the M.S. degree in Information Engineering University. His research interests include radar detection and signal processing.

Dexiu Hu received the B.S. and M.S. degrees from the Zhengzhou Information Technology Institute, Zhengzhou, China, in 2007 and 2010, respectively, and the Ph.D. degree in electronic engineering from Tsinghua University, Beijing, China. He is currently an associate professor with Information Engineering University, Zhengzhou, China. His current research interests include radar signal processing and passive location.